MINISTRY OF EDUCATION AND TRAINING
VIETNAM ACADEMY OF SCIENCE AND TECHNOLOGY
ACADEMY OF SCIENCE AND TECHNOLOGY

Vu Duy Thinh

RESEARCH AND PRODUCTION OF ENVIRONMENTAL TREATMENT AND CO_2 CONVERT OF CO_2 INTO FUEL GAS

Specialization: Electronic Materials
Code: **9.44.01.23**

SUMMARY OF THE DISCUSSION OF MATERIALS SCIENCE

Hanoi –2023

The work was completed at: Academy of Science and Technology - Vietnam Academy of Science and Technology.

Science instructor 1: Dr. Ngo Thi Hong Le
Science instructor2: Prof. Dr. Vu Dinh Lam

Review 1:.....

Review2:.....

Review 3:.....

The thesis was defended in front of the Academy-level Doctoral Thesis Evaluation Council, meeting at the Academy of Science and Technology - Vietnam Academy of Science and Technology at ... hour ..', date ... month ... year 2023

The thesis can be found at:

- Library of Academy of Science and Technology
- Vietnam National Library

PREAMBLE

Currently, all of humanity is facing serious environmental problems such as water pollution, air pollution, global warming, energy shortage and problems related to climate change. Photocatalysis will treat water, air, organic pollutants through redox reactions and allow direct conversion of solar energy into chemical energy for water splitting and hydrogen production, or photoreduction of CO_2 into useful organics and fuel gases. TiO_2, ZnO materials under the effect of light act as a bridge to transfer electrons from H_2O to O_2 (provided by the external environment) converting these two substances into O_2 - and OH * forms. are two types of substances with high oxidizing activity capable of decomposing organic matter. At the same time, the TiO_2 and ZnO substrates are also used for the CO_2 photoreduction process which have been studied the most because they are stable, non-toxic and have low cost.

However, these two materials have a large band gap (3.2eV for TiO_2, 3.3 eV for ZnO), so they can only absorb ultraviolet light and have a fast electron-hole recombination rate. reduce the efficiency of the photocatalysis. To obtain high photocatalytic activity for this material in the visible light region, the structure, size and shape of TiO_2 and ZnO have been modified by using different fabrication methods., doping or attaching other elements... to reduce the band gap, shift the absorption wavelength to the visible light region, and reduce the probability of electron-hole recombination.

In Vietnam as well as in the world, scientific researches on TiO_2, ZnO are quite numerous, focusing mainly on the fabrication of TiO_2, nano-sized ZnO oriented for application in environmental treatment and TiO fabrication research.2, ZnO modified by physical and chemical methods. However, so far, studies on co-doped and heterodoped TiO_2, ZnO systems as well as electron transfer mechanisms in these materials have not been presented and reported more explicitly. Besides, studies on the application of these materials in CO_2 photoreduction to generate fuel gas in Vietnam are still relatively new. Therefore, in order to catch up with the trend of

catalyst development, the content I chose to conduct the thesis is: Research on fabrication of *TiO_2 photocatalysts, application-oriented modified ZnO for environmental treatment and conversion. convert CO_2 into fuel gas"* .

The aim of the thesis:

Successful synthesis of photocatalytic materials TiO_2, modified ZnO is effective for the decomposition reaction of toxic organic compounds in water for application in environmental treatment and conversion of CO_2 into fuel gas

To achieve the set objectives, we have implemented the following specific research contents:

+ Research on fabrication of TiO_2 nanoparticles and TiO_2 nanowires, N, Ta doped TiO_2 nanoparticles by hydrothermal method. Study on fabrication of Ag/TiO_2 nanowire materials by photoreduction method using UVA lamp.

+ Research on fabrication of ZnO films and ZnO nanowires by hydrothermal method. Study on fabrication of Au-Ag-ZnO film materials and CuO-Ag-ZnO nanowire materials by plasma technique.

+ Investigate the influence of technological conditions on the photocatalytic activity and the photocatalytic performance of CO_2-generating methane gas of the materials.

CHAPTER 1. OVERVIEW

1.1 TiO_2 and ZnO . photocatalyst materials

In nature TiO_2 exists in 3 phases: rutile, anatase, brookite with definite color and crystal shape. Pure can TiO_2 phase rutile and anatase even Have structure bamboo quartet sense (tetragonal) and Okay build build from the Multi face mix wisdom bowl face (octahedra), in each bowl face Have first ion Ti^{4+} lie live heart and 6 ion O^{2-} lying live 2 top and 4 corner. Degree wide region ban and structure bamboo the level power quantity miscellaneous matter in region ban dependent enter the needle type Okay doping enter TiO_2 . Degree wide region ban Eg belong to anatase and rutile TiO_2 forms block soy sauce application To be 3,2 eV and 3,0 eV equivalent application with power quantity photon in region ray death foreign (UV) Have step wave 387 nm and 410 nm.

ZnO belong group semiconductor _ A^{II} B^{VI}’ Have 3 form structure bamboo: hexagonal wurtzite, zin blende, rocksalt. In there, structure bamboo hexagonal wurtzite To be structure bamboo durable, thermally stable should be the structure spectrum most variable. At the structure wurtzite, each atom oxygen contact conclude with 4 original death zinc and reverse again. ZnO To be sell guide type n, degree wide region ban 3,4 eV live 300K. ZnO pure pure To be matter way electricity, live heat degree short. Below bottom region guide exist in2 level donor way bottom region guide time in turn is 0,05 eV and 0,15 eV. LIVE normal temperature, electrons are not capable enough quantity to dance go up region guide. Because So, ZnO guide electricity least at heat degree room. When heat degree increase arrive about200^oC - 400^oC, the electronic receive Okay energy _ heat enough big they Have can move transfer go up region guide, at the time there ZnO return wall matter guide electricity. ZnO also Have count matter optical contact works soy sauce on one's own like TiO_2 . Although of course, ability optical contact works belong to ZnO weak than so with TiO_2 .

1.2 Photoreduction process

CO_2 photoreduction is hypothesized to follow the following three steps: (i). Excitation of the band gap to generate photogenerated electron-hole pairs; (ii). Separation and displacement of electron carriers; (iii). Reduction of CO_2 and reduction of H_2O by photoelectrons. During photoreduction of CO_2 and separation of H_2O, light hitting the photocatalyst surface creates electron-hole pairs in TiO_2 or ZnO. Electrons are excited in the conduction band of TiO_2, ZnO can migrate to the surface and reduce CO_2 to fuel (CH_4, CH_3OH, HCOOH...). Meanwhile, the hole left in the valence band of the semiconductor photocatalyst can oxidize water to oxygen gas .

1.3 Methods for making nano-sized materials

Recently, there are many methods to synthesize nano-sized materials such as sol-gel method, hydrothermal method, microwave method, co-precipitation, mold synthesis (hard mold, soft mold).), and methods with the effect of physical agents such as isostatic heating, microwave heating, ultrasonic vibration, low pressure, high pressure, etc., are used to create nanostructures. different lows. In it, Microwave material synthesis offers high efficiency and selectivity for the synthesis of porous materials. However, this method has a very high equipment cost, so this method is not widely applied. In addition, the microwave method is initially used in the synthesis of inorganic nanomaterials and there is still a long way to go. quite far from its potential . However, the rapidly growing number of publications in this field suggests that the microwave method will play a prominent role in the vast field of nanoscience and technology. The extent to which improvements in microwave technology can affect particle growth and allow these processes to be commercialized is currently not well defined.

1.4. Overview of materials TiO_2, ZnO modified

To expand the application range of semiconductor photocatalytic materials TiO_2, ZnO, these materials are often modified by different methods such as doping metal or non-metal ions, surface sensitization by organic molecules or metal complexes,

deposition of metal oxide materials with small band gap or metal materials on the surface . Metals doped into TiO_2 semiconductor materials include alkali metals, alkaline earth metals (Na, K, Li, Mg, Ca) and transition group metals (Au, Ag, Pt, V, etc.) W, Nb, Ce, Sn, Zr, Cr) . The properties of modified TiO_2 materials depend on the nature, properties, and content of the doping element and the method of modification . These metals change the optical activity, electron–hole recombination rate, and surface electron transfer rate. When doping TiO_2 materials with non-metallic elements (N, F, C, S, I, F) will reduce the band gap, shifting from the UV radiation region to the visible region . In order to increase the photocatalytic activity of TiO_2 materials under visible light, it is also performed (optically) to sensitize the TiO_2 surface by organic molecules or metal complexes.

ZnO has a band gap energy similar to TiO_2 (3,2 eV) and has many properties such as high chemical stability, non-toxicity, low cost, abundant in nature, so ZnO materials are still used by scientists. care about. And to increase the photocatalytic activity, ZnO has been doped by more metal atoms or metal oxides to reduce the band gap energy and reduce the recombination of the photogenerated electron-hole pair.

CHAPTER2: US EXPERIENCE AND RESEARCH METHODS

2.1. Equipment and tools

– The processes of synthesis, research and manufacture of the thesis are carried out mainly at the Institute of Materials Science - VAST.

– In addition, the equipment and instruments are used at prestigious scientific research facilities in Vietnam.

2.2. Chemicals and materials .

Chemicals from high quality chemical firms such as Merck (Germany), Sigma (USA), ... are used for research, manufacturing, measurement, evaluation and calculation in the thesis.

2.3 Fabrication of TiO_2 nanoparticles, TiO_2 nanowires and Ag/TiO_2 nanowires

TiO_2 was prepared by a two-step hydrothermal method. Step 1 is to synthesize TiO_2 nanoparticles by hydrothermal method at 200^{o}C for 24 hours using the precursor Tetraisopropyl orthotitanate (TPOT). Then, step 2 is that TiO_2 nanowires synthesized from TiO_2 nanoparticles in step one are further hydrothermally in 10M KOH alkaline solution at 180 ^{o}C for 24h .

2.4 Fabrication of TiO_2, N-doped TiO_2 and co-doped (N, Ta) crystals by hydrothermal method

crystals, the solution to be prepared for hydrothermal process consists of TPOT dissolved in IPA in deionized water and NH_4OH and for the preparation of co-doped (N, Ta) TiO_2 powders.), the solution to be prepared for hydrothermal process consists of TPOT dissolved in IPA dissolved in deionized water, NH_4 OH and Ta (HNO_3 + HF).

2.5 Fabrication of TiO_2, N-doped TiO_2 and TiO_2 (N, Ta) powder by microwave method

2.6 Fabrication of Ag and Au-doped ZnO films by plasma technique

Hydrothermal, photoreducing and plasma techniques for film fabrication. The hydrothermal method was used to synthesize ZnO

film materials on glass substrates. To fabricate the Ag-ZnO film material, the plasma electrolytic oxidation method is used to coat the Ag nanoparticles on the ZnO film. Then, using photoreducing $HAuCl_4$ acid to Au nanoparticles coated on Ag/ZnO film.

2.7 Fabrication of ZnO, Ag/ZnO and CuO-Ag-ZnO nanowires by hydrothermal and plasma techniques

The ZnO wire material was fabricated by hydrothermal method and the PEO method was used to attach Ag and CuO nanoparticles onto the ZnO nanowire.

2.8 Research methods to evaluate the properties of fabricated materials

X-ray diffraction measurements, scanning electron microscopy (SEM), transmission electron microscopy (TEM), UV-vis absorption spectrometry, Raman measurements, Fourier infrared spectrometry (FT-IR), fluorescence spectrometry, chromatography, energy dispersive X-ray spectroscopy (EDX), nitrogen adsorption - desorption isotherm (BET) method. . is used in this thesis to study and evaluate the properties of fabricated materials. The main measurement methods are measured at VAST Institute of Materials Science, and prestigious scientific research facilities. At Hanoi.

2.9 Research method for photocatalytic reaction and photoreduction of CO_2

In the thesis, the photocatalytic reaction was carried out through the ability to decompose methyl dacam, methylene blue and Rhodamine under the light of Xenon lamp with a power density of 100 mW/cm^2 (Solar Simulator: Oriel Sol 1A) . wavelength range from the ultraviolet to the infrared region.

The photocatalytic reduction experiment was carried out in a glass flask placed on a magnetic stirrer: The powder sample and deionized water were placed in the reaction vessel. CO_2 was passed through the reactor about 1 hour before illumination. The light source is a 250W mercury lamp with a spectrum similar to that of sunlight. The CO_2 reduction photocatalytic reaction was carried out for 5 h at room temperature. At the end of the reaction, the gas sample was withdrawn using a syringe and analyzed on a gas chromatograph.

CHAPTER 3 : RESEARCH OF FACILITATION AND CO_2 photocatalytic activity and photocatalytic activity of Ag/TiO_2 AND TiO_2 : (N, Ta)

3.1. CO_2 photocatalytic activities of Ag/TiO_2 . nanowires

Figure 3.1(a) shows that TiO_2 has a nanowire structure with a diameter of less than 50 nm and a length of about 600 nm. After TiO_2 nanowire was attached with Ag nanoparticles by photoreduction method, Ag/TiO_2 in SEM image Figure 3.1(b) showed a clear appearance of Ag particles with size of about 5-10 nm. evenly coated on the surface of TiO_2 nanowires . Figure 3.2 is the X-ray diffraction pattern of TiO_2 and Ag/TiO_2, the TiO_2 nanowire has the corresponding X-ray diffraction pattern that coincides with the titanate structure $H_2Ti_3O_7$. After the Ag nanoparticles were attached to the TiO_2 nanowire by photoreduction method, the TiO_2 nanowire structure had a clear change from the titanate phase to the anatase and rutile phase. From the XRD results, it was shown that TiO_2 nanowires with titanate crystalline phase structure were successfully synthesized by hydrothermal method, after the Ag nanostructure was coated on the above TiO_2 structure, the presence of Ag was demonstrated in the XRD diagram and can be the agent to increase the crystallinity of TiO_2 wire to a more stable phase structure.

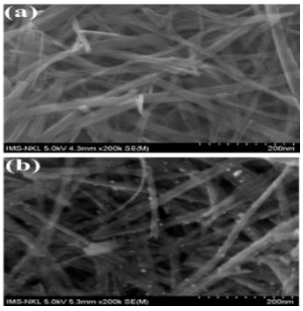

Figure 3.1 : FESEM images of (a) TiO_2 and (b)Ag/TiO_2

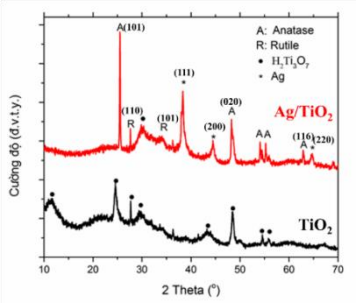

Figure 3.2: X-ray diffraction pattern of two samples TiO_2 and Ag/TiO_2

Figure 3.3 is the UV-Vis absorption spectrum of TiO_2 and Ag/TiO_2 nanowires showing, Compared with the original TiO_2 nanowire sample, the Ag nanoparticles mounted on the TiO_2 nanowire surface significantly increased the photon absorption

capacity and extended the absorption region of the Ag/TiO_2 nanowire sample to the light region. visible light (410 nm) . At the same time, on the absorption spectrum of Ag/TiO_2, there is an absorption peak at the wavelength position 418. nm, this absorption peak corresponds to the plasmon peak of Ag. The The significant enhancement of the optical properties of Ag/TiO_2 compared with that of TiO_2 was initially thought to be the result of the local surface plasmon effect of the Ag nanoparticles. From this result, it shows that the ability of TiO_2 to absorb light in the visible light region when adding Ag nanoparticles has been significantly increased, thereby contributing to the increased activity of Ag/TiO_2 materials in optical applications.

Figure 3.4 shows the decomposition efficiency of Methyl Orange (MO) according to different lighting times of TiO_2 and Ag/TiO_2 wires . MO decomposition efficiency of TiO_2 nanowires was 69,3%, but when the Ag nanoparticles were attached, Ag/TiO_2 showed effective MO decomposition efficiency and increased significantly with 98,8%.

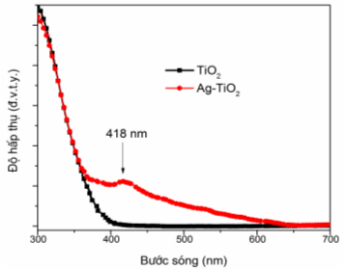

Figure 3.3: UV-vis absorption spectrum of TiO_2 and Ag-TiO_2 . nanowires

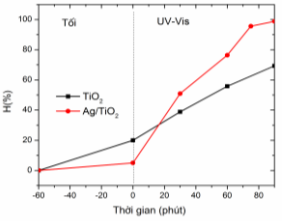

Figure 3.4: Decomposition efficiency of Methyl Orange (MO) with different lighting time of TiO_2 and Ag/TiO_2 wires

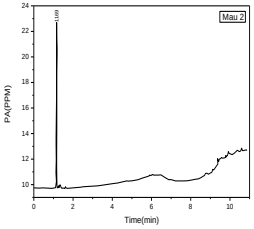

Figure 3.5 : The obtained chromatogram of the Ag/TiO_2 . nanowire

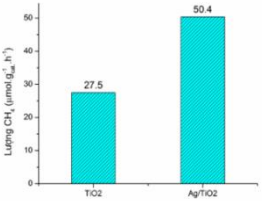

Figure 3.6 : Comparison chart of CH_4 gas per 1g catalyst in 1 hour after photoreduction of CO_2 by UVA light of TiO_2 and Ag/TiO_2 wires

Ag/TiO_2 was studied for its ability to photoreduce CO_2 to form CH_4 gas . From the chromatogram in Figure 3.5, it can be seen clearly and uniquely that at a retention time of 1.169 minutes, a gas peak appears corresponding to CH_4 gas . This result confirms that the Ag/TiO_2 nanowire is capable of photoreducing CO_2 to CH_4 with high selectivity. Figure 3.6 is a comparison chart of CH_4 gas per 1g catalyst in 1 hour of TiO_2 and Ag/TiO_2 wires . The amount of CH_4 gas from the photoreduction of CO_2 of TiO_2 is 27,5 µmol.g $^{-1}$ cat.h $^{-1,}$ while that of the Ag/TiO_2 nanowires has been increased almost twice to 50,4 µmol.g $^{-1}$ cat.h $^{-1}$.

3.2 Fabrication and study of photocatalytic activity of TiO2, N-doped TiO_2, co-doped TiO_2 (N, Ta)

X-ray diffraction pattern to determine the structure and phase composition of TiO_2 (green), N doped TiO_2 (blue) and N, Ta co-doped TiO_2 (red) . The diffraction peaks are studied and correspond to planes (101), (013), (004), (112)..., indicating that the fabricated samples have anatase phase structure (JCPDS tag21). -1272). Besides, from the X-ray diffraction pattern at the small angle position, a small change in the diffraction peaks between the TiO_2 samples and the doped TiO_2 samples is observed. This shows a change in the anatase structure when the TiO_2 nanoparticles are doped with N and co-doped (N, Ta).

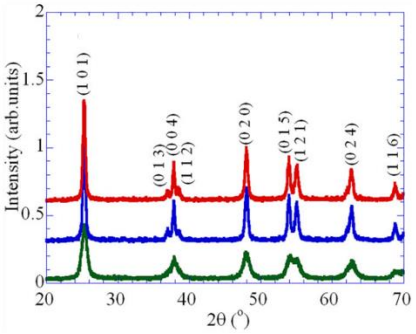

Figure 3.7: (a) X-ray diffraction pattern of samples TiO_2 (green), N-doped TiO_2 (blue) and co-doped TiO_2 (N, Ta) (red)).

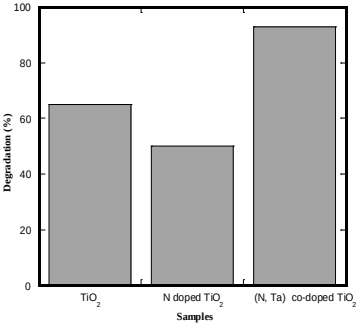

Figure 3.8 : MB decomposition efficiency of N-doped TiO_2, N - doped TiO_2 and co-doped (N, Ta) TiO_2 in 180 minutes.

Along with that, the Raman spectra of the samples all have five peaks at positions 145 $cm^{-1,}$ 196 $cm^{-1,}$ 398 $cm^{-1,}$ 516 cm^{-1} and 640 cm^{-1} . In which the peaks at position 145 $cm^{-1,}$ 196 cm^{-1} and 640 cm^{-1} correspond to the Eg mode of TiO_2 anatase phase and the 2 peaks at the position 398 $cm^{-1,}$ 516cm^{-1} respectively. with mode B_{1g} and mode B_{1g} /A_{1g} of TiO_2 phase anatase. This result is consistent with the XRD results discussed above. From the SEM images of the fabricated $TiO_{2,}$ N-doped TiO_2 and co-doped (N, Ta) TiO_2, it is shown that all TiO_2 and TiO_2 have N-doped and co-doped (N, Ta) are uniform. structures with an average diameter of 15–25 nm. The average nanoparticle size is estimated to be less than20 nm for pure TiO_2 and co-doped TiO_2 (N, Ta). Meanwhile, N-doped TiO_2 has an average grain size larger than20 nm. The surface area of $TiO_{2,}$ N-doped TiO_2 and co-doped TiO_2 (N, Ta) samples are estimated to be 145,5, respectively; 59,0 and 109,5 m^2/g.

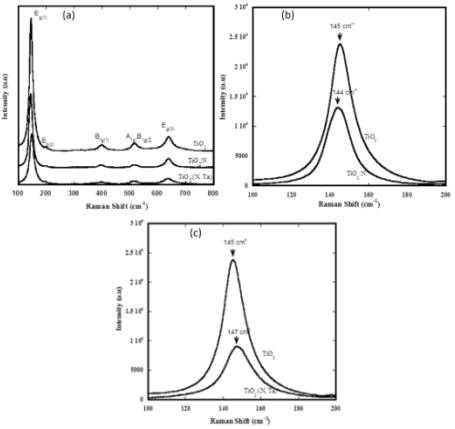

Figure 3.9 : (a) Raman spectra of $TiO_{2,}$ N-doped TiO_2 and co-doped TiO_2 (N, Ta); (b) Raman spectra at E_g mode of the N-doped TiO_2 and TiO_2 samples ; (c) Raman spectra at Eg mode of the N co-doped TiO_2 and TiO_2 samples, Ta

In Figure 3.8, visible light photodegradation, undoped TiO_2 exhibits rather poor photocatalytic activity, only 65% of the original methylene blue decreased after 180 min. By doping N into $TiO_{2,}$ the photodegradation rate was reduced to 50% after 180 min, this result is because the N-doped TiO_2 has the lowest surface area among the 3

fabricated samples. In particular, the co-doped TiO_2 (N, Ta) has the highest photocatalytic activity of all the compared materials. For this sample, 93% of the tested methylene blue decomposed within 180 min of illumination.

3.3 Fabrication and study of photoreduction of CO_2 into CH_4 fuel gas of co-doped TiO_2 (N, Ta) with different mass percentages of N by microwave method.

Study the effect of co-doping (N, Ta) with different mass percentages of N (with 4 mass percentages of 6%, 7,5%, 9% and 10,5%. together with 0,5%Ta constant) to the crystal structure, morphology and optical properties of TiO_2 . With 4 percentages of mass N increasing respectively with the symbols TN1Ta, TN2Ta, TN3Ta, TN4Ta, respectively.

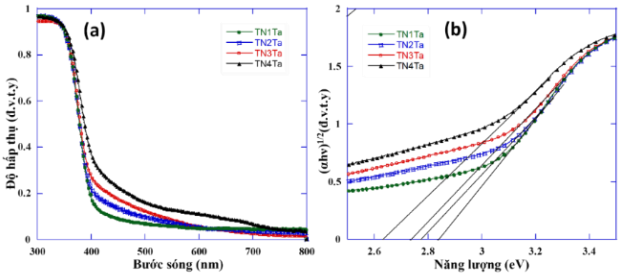

Figure 3. 10 : (a) Absorption spectrum and (b) The dependence of (α hν) 1/2 on the photon energy (hν) of the samples TN1Ta, TN2Ta, TN3Ta, TN4Ta

From SEM and XRD image results, TN1Ta, TN2Ta, TN3Ta, TN4Ta fabricated are modified TiO_2 with anatse phase structure with particle size of about 10-25 nm. From the absorption spectrum figure 3. 10 In the visible light region, the absorption coefficient of semiconductor materials (α) is calculated according to the formula $\alpha h\nu = A_1(h\nu - Eg)^{1/2}$ for straight bandgap semiconductors and $\alpha h\nu = A_2(h\nu - Eg)^2$ for the biased band gap semiconductor .

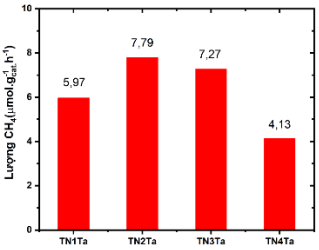

Figure 3: 11: Chart of the amount of CH4 gas obtained after the visible light CO_2 photoreduction process of samples TN1Ta, TN2Ta, TN3Ta, $_{TN4Ta}$

The results of gas chromatography measurement of samples TN1Ta, TN2Ta, TN3Ta, TN4Ta are shown in Figure 3.16. From the measurement results, we can see that sample TN2Ta gives the highest concentration of CH_4 gas at 7.79 µmol.g^{-1} cat.h^{-1} while sample TN4Ta gives the smallest concentration of CH_4 gas at 4.13 µmol.g^{-1} cat.$h^{-1,}$ next to *TN1Ta, TN3Ta give* CH_4 gas concentrations of 7.27 µmol.g^{-1} cat.h^{-1} and 5.97 µmol.g^{-1} cat.$h^{-1,}$ respectively. Although doped with a smaller concentration of N, has a larger band gap, but in the TN2Ta sample, there is a concordance of Ta^{5+} and N^{3-} ions, making the lattice cell volume the smallest in the samples. along with the existence of many electron-hole pairs, therefore, TN2Ta with 7.5% N doped shows the best ability to photoreduce CO_2 to CH_4 fuel gas .

CHAPTER 4: RESEARCH OF FACILITATION AND PHOTOCELACTACTICAL ACTIVITIES OF SOME ZnO BACKGROUND MATERIALS

4.1 Fabrication and study of photocatalytic activity of Ag-ZnO and Au-Ag-Zn . films

ZnO film (symbol Z0) was synthesized by spin coating method combined with hydrothermal on glass substrate. ZnO film coated with Ag nanoparticles by plasma technique with2 concentrations of AgNO3 precursors, 5mM and 45mM, produces two film products with symbols Zp-Ag5 and Zp-Ag45, respectively. Then Au nanoparticles were attached to the two upper films by redox method to produce Au-Zp-Ag5 and Au-Zp-Ag45 products. In addition, to compare the ZnO product coated with Au nanoparticles was also synthesized and studied, denoted as Au-Z0 .

Scanning electron microscopy (SEM) images were used to study the morphology of the prepared Z0, Zp-Ag5 and Zp-Ag45, Au-Z0, Au-Zp-Ag5, Au-Zp-Ag45 films and The results of SEM images of the surface and cross-sectional SEM images are obtained in Figure 4.1. First, the SEM image of Z0 in Figure 4.1(a) shows that the fabricated Z0 material has the form of vertically aligned nanorods with an average diameter of about 500 nm. The thickness of this ZnO film is about 3.1 μm (Figure 4.1 g). When Ag nanoparticles were coated onto ZnO films with AgNO3 precursor concentrations of 5 and 45 mM by plasma technique, the surface of the material became rough with many hexagonal cavities, and the number of cavities also increased., as shown in Figures 4.1(b) and (c). In addition, the film thicknesses of Zp-Ag5 and Zp-Ag45 were significantly reduced to 1.91 μm and 1.51 μm, as shown in Figure 4.1 (h, i). The size of the Ag nanoparticles in Zp-Ag5 is about 5–30 nm and the size of the Ag nanoparticles in Zp-Ag45 is much larger around 10–50 nm. From the SEM images, it shows that the plasma process and different AgNO3 concentration are important factors affecting the morphology of the film as well as the size of Ag in the ZnO material system modified by attaching Ag nanoparticles [112].][113]. Then, Zp-Ag5 and Zp-Ag45 films were

coated with Au nanoparticles by photoreduction method, their surface became porous with the appearance of Au nanoparticles with size from20 to 30 nm, figure 4.1 . (DF). Cavities formed on ZnO films can anchor Au nanoparticles on the membrane surface. From the SEM image, it can be clearly seen that the formation of ZnO and Ag, Au has been successfully attached to the ZnO film.

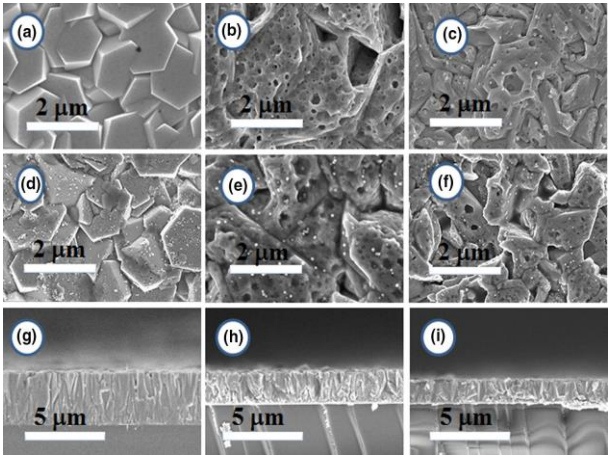

Figure 4.1 : SEM images capture the surface of (a) Z0, (b) Zp-Ag5, (c) Zp-Ag45, (d) Au-Z0, (e) Au-Zp-Ag5, (f) Au-Zp-Ag45 and cross-sectional SEM images of (g) Z0, (h) Zp-Ag5, (i) Zp-Ag45

The X-ray diffraction pattern of samples Z0, Zp- Ag5 and Zp-Ag45 shows that there are four diffraction peaks at the angular position of 31,8^{o} ; 34,4^{o} ; 36,3 and 47,6^{o} . These diffraction peaks are compared and completely coincide with the (100), (002), (101) and (102) planes of ZnO wurtzite (JCPDS tag number 36-1451), respectively. No characteristic diffraction peaks were observed for Ag metal, which may be due to the low concentration of AgNPs. Furthermore, observing the highest peak at the angular position 34,43^{o} corresponding to the (002) plane, the intensity of the peak for Z0, Zp-Ag5 and Zp-Ag45 films gradually decreased, respectively. As mentioned in the cross-sectional surface SEM results, the thicknesses of Z0, Zp-Ag5 and Zp-Ag45 decreased, so the amount of Z0 in Zp-Ag5 and Zp-Ag45 decreased and their diffraction intensity also decreased.

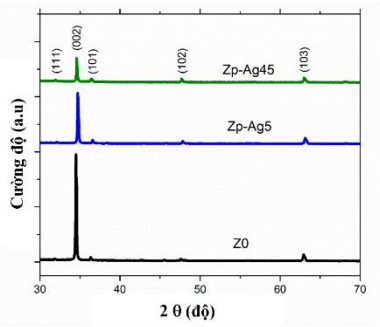

Figure 4.2: X-ray diffraction pattern of Z0, Zp-Ag5 and Zp-Ag45

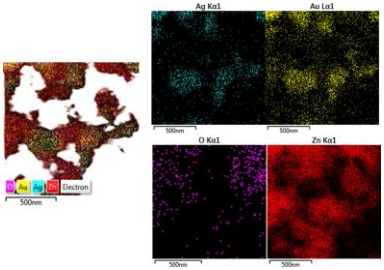

Figure 4. 3 : STEM mapping image (map of O, Au, Ag, Zn atoms) in Au-Zp-Ag45 sample

To study the chemical composition of the fabricated materials, Au-Zp-Ag45 is represented to measure STEM-mapping. The STEM-mapping image (atomic diagram O, Au, Ag, Zn) in the Au-Zp-Ag45 sample is shown in Figure 4.3. From the STEM results, it is shown that Au-Zp-Ag45 has the chemical compositions of O, Zn, Ag and Au. Along with that, the very uniform distribution of O, Au, Ag, Zn atoms in the Au-Zp-Ag45 sample can be easily observed. The Tauc plot of *(ahv)2* versus *hv* is shown in Figure 4.4(b). The band gap (Eg) values $_{of}$ the fabricated samples are listed in Table 4.1. It can be seen that the bandgap widths of Z0, Zp-Ag5 and Zp-Ag45 films increase from 2,94 eV to 3,2 eV when the film thickness is reduced from 3.1 μm to 1,51 μm. The film thickness has a strong influence on the band gap of ZnO films [116], the band tends to narrow as the film thickness decreases and the absorption spectrum tends to shift to the red light region. for thicker films. This shift is mainly due to the change in carrier concentration. In this case, an increase in Ag concentration, a decrease in film thickness, could be one of the factors causing a shift to the blue light region of the absorption spectrum [116].

The calculated bandgaps of Au-Z0, Au-Zp-Ag5 and Au-Zp-Ag45 are 2,88 eV, 2.99 eV and 3,14 eV, respectively, and are shifted

to the red light region times compared with Z0, Zp-Ag5 and Zp-Ag45. This shift can be attributed to the electron transfer between Au nanoparticles and the optical transition in the ZnO film.

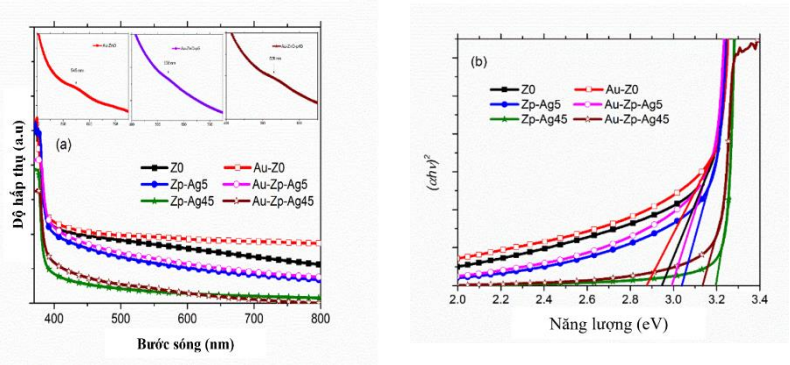

Figure 4. 4 : a) Absorption spectra of samples Z0, Zp-Ag5, Zp-Ag45, Au-Z0 Au-Zp-Ag5 and Au-Zp-Ag45, with the insets in the figure being the absorption spectrum of the samples. Au-Z0, Au-Zp-Ag5 and Au-Zp-Ag45; (b) Tauc plot to calculate band gap of samples

Figure 4.5 shows the fluorescence (PL) spectrum of samples Z0, Zp-Ag5, Zp-Ag45, Au-Z0, Au-Zp-Ag5 and Au-Zp-Ag45 excited by laser light with wavelength. 355 nm. The PL spectra of the samples showed strong near band gap Energy (NBE) and very weak wide visible region (Vis) emission due to DLE (deep level emission) from intrinsic and extrinsic defects. . Since the energies of the NBE and DLE are often in competition with each other, this usually reduces the defect centers so that the UV region emission in the PL spectrum can be enhanced. As can be seen from Figure 4.5, the UV region emission intensity in the PL spectrum of Zp-Ag45 is about 1.2 and 3.9 times higher than that of Zp-Ag5 and Z0 films, respectively. Samples doped with Au, Au-Z0, Au-Zp-Ag5 and Au-Zp-Ag45 show only the UV region emission spectrum and the Vis region emission spectrum almost disappears. The enhancement of UV emission in the PL spectra of Zp-Ag5 and Zp-Ag45 films can be attributed to the doping of Ag nanoparticles on ZnO, which increases the number of excited carriers and improves the recombination rate. radiation [116][118].

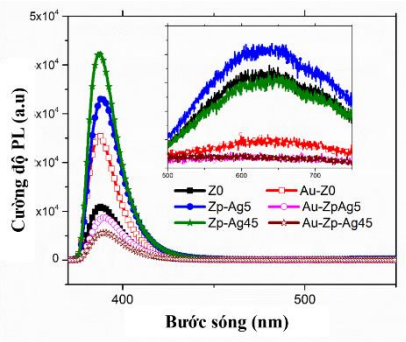

Figure 4.5 : Fluorescence (PL) spectra of the fabricated samples Z0, Zp-Ag5, Zp-Ag45, Au-Z0, Au-Zp-Ag5 and Au-Zp-Ag45; Inner inset is PL spectral magnification of samples in Vis region (visible light region)

In the case of Au-Z0 sample, the UV emission intensity in the PL spectrum is enhanced by about 2,35 times that of Z0. The intensities of Au-ZpAg5 and Au-Zp-Ag45 were reduced by about 3,67 and 7,3 times, respectively, compared with Zp-Ag5 and Zp-Ag45. In fact, depending on the band structure of the semiconductor and metal, as well as the emission energy state, the energy or electron transfer from the metals - the semiconductor and the PL emission can be increased. strong. If the energy or electrons move in the opposite direction, the PL emission spectrum is extinguished. In this study, the conduction band, valence band and deep-defect level of ZnO are at 4,19 eV; 7,39 eV and 5,09 eV. The Fermi energy level of Au is 5.1 which is close to the deep vacancy level of ZnO. This allows the defect-related electron flow from ZnO to be transferred to the Fermi level of Au. Electrons from the Fermi level lead to the appearance of surface plasmon resonance (SPR) in Au particles excited to a high energy state, which can jump into the conduction band of ZnO. Thus, the PL intensity of the UV emission is enhanced and the emission associated with the defect region is suppressed. If defect-related emission could be prevented in such a way, this would lead to enhanced emission in the ultraviolet region and enhanced recombination rate of electrons and holes, leading to decreased photocatalytic activity in Au-Z0 films.

As mentioned above, the band gap of Zp-Ag5 or Zp-Ag45 is larger than that of Z0. Therefore, the working region of ZnO can be higher than the Fermi level of Au (5.1 eV). As a result, whenever there is contact between ZnO and Au, electrons from the conduction band of ZnO can be transferred to AuNPs. The mechanism used to account for UV emission in the PL spectrum is significantly reduced in Zp-Ag5 or Zp-Ag45. In addition, the Au nanoparticles introduced into the material system can trap the photogenerated electrons, prevent their recombination with holes as well as enhance the photocatalytic activity.

Degradation of pollutants by Au and Ag nanoparticles on ZnO films has been reported by various groups (table 4.1).

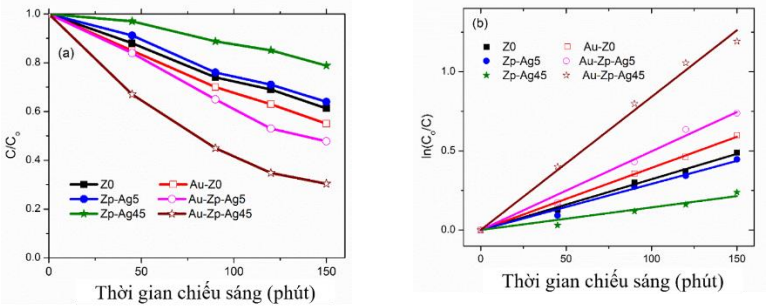

Figure 4.6 : Kinetics of RhB photodegradation by samples Z0, Zp-Ag5, Zp-Ag45, Au-Z0, Au-Zp-Ag5 and Au-Zp-Ag45; (b) Corresponding curve of the function ln (C /Co) with time during RhB . decomposition

Table 4.1: Decomposition efficiency table and k-first order kinetic energy constant of the fabricated materials Z0, Zp-Ag5, Zp-Ag45, Au-Z0, Au-Zp-Ag5 and Au-Zp-Ag45 in the degradation of Rhodamine B (RhB).

Form name	Decomposition efficiency (%)	*k-first order kinetic energy constant*
Z0	38	0,0 0 32
Zp-Ag5	36	0,0 02 9
Zp-Ag45	21	0,0 0 1 4
Au-Z0	45	0,0 0 3 9
Au-Zp-Ag5	52	0,0 0 4 9
Au-Zp-Ag45	70	0,0 0 8 4

4.2 Fabrication and study of photocatalytic activity of ZnO, CuO-Ag-ZnO in methyl orange decomposition

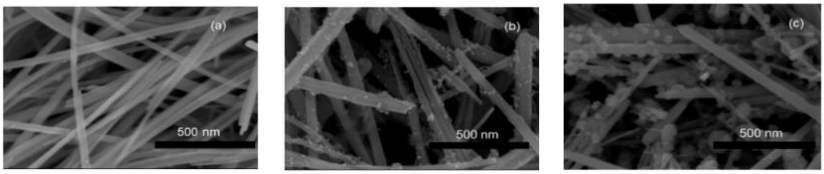

Figure 4. 3: SEM nanowires (a) ZnO, (b) Ag-ZnO, and (c) CuO-Ag-ZnO

Figure 4.3(a) is a snapshot of the surface structure of smooth surface ZnO nanowires with a diameter between ~20–70 nm. Figure 4.3 (b), (c) shows the turn FE-SEM images of ZnO nanowires added by Ag nanoparticles, and Ag and CuO nanoparticles, respectively, using plasma process. Compared with ZnO nanowires, the successful deposition of nanoparticles on the surface of ZnO NWs can be confirmed.

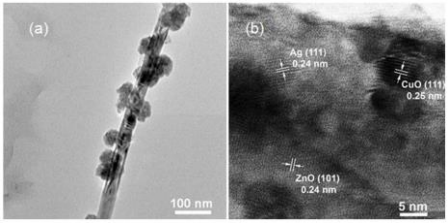

Figure 4.4: TEM Figure (a) and HRTEM (b) of NW CuO-Ag-ZnO.

Figure 4.4 depicts TEM and HRTEM images of CuO-Ag-ZnO NWs. The obtained TEM images show the occupation of Ag and CuO NF NPs on the surface of the ZnO nanowire. HRTEM image analysis (Figure 4.4(b)) confirmed the co-existence of the crystalline lattices of ZnO, Ag and CuO.

In the X-ray diffraction pattern of the ZnO, Ag-ZnO and CuO-Ag-ZnO NWs, all the sharp peaks in the pattern coincide with the X-ray diffraction pattern of the hexagonal wurtzite structure of ZnO. The characteristic diffraction peaks of ZnO NWs with the growth direction along the c-axis observed on all samples correspond to the typical ZnO wurtzite crystal structure. There was no peak change indicating that the Ag and CuO NF nanoparticles nor the plasma treatment damaged or affected the original ZnO crystal structure.

In addition, the activity functions of CuO, ZnO and Ag NPs are around – 4,07, - 4,35 and – 4,26eV on the absolute vacuum scale, respectively. Electrons from the Fermi level can also move into the conduction band of ZnO. As a result, the PL intensity decreased in both UV and VIS emission, leading to a significant inhibition of the electron-hole recombination rate and thus markedly improving the photocatalytic degradation of the catalyst. .

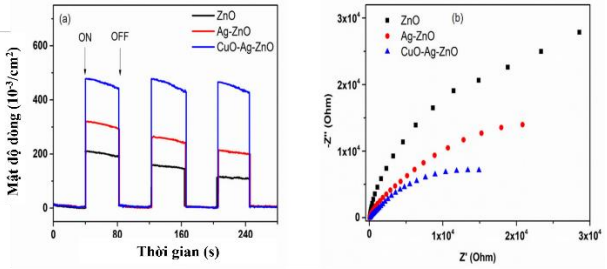

Figure 4.5 : (a) Photocurrent-time density curves of ZnO, Ag-ZnO and CuO-Ag-ZnO under illumination/unilluminated (on/off) of simulated light sunlight and (b) Nyquist plots of ZnO, Ag-ZnO and CuO-Ag-ZnO.

The electron and hole separation efficiency in semiconductors has a great influence on the photocatalytic activity. Figure 4.5 (a) shows the photocurrent-time-density curves of the ZnO, Ag-ZnO and CuO-Ag-ZnO photoelectrodes

The photocatalytic activities of ZnO, Ag-ZnO and CuO-Ag-ZnO samples were investigated by monitoring the change of the maximum absorption peak of the MO dye at 465 nm. The intensity of the absorption spectra decreased markedly with increasing irradiation time and the peak position was shifted to the left, after the MO dyes were optically degraded.

Figure 4.6(a) shows the relationship between C_t /C_0 decomposition and irradiation time, the CuO-Ag-ZnO NWs clearly have the highest photocatalytic activity and about 100% MO can be degraded. decomposes within 30 minutes after irradiation by sunlight. The NWs with Ag-ZnO and ZnO had

lower photocatalytic activity, in which about 98.5% and 89% of MO were photodegraded within 30 min, respectively.

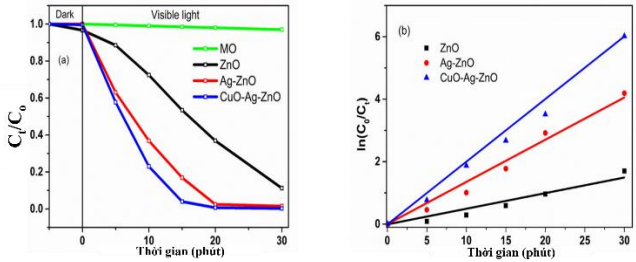

Figure 4. 6 (a) Kinetics of MO photodegradation by ZnO, Ag-ZnO and CuO-Ag-ZnO samples and (b) Curve of ln function (C/Co) with corresponding time for the photodegradation of MO.

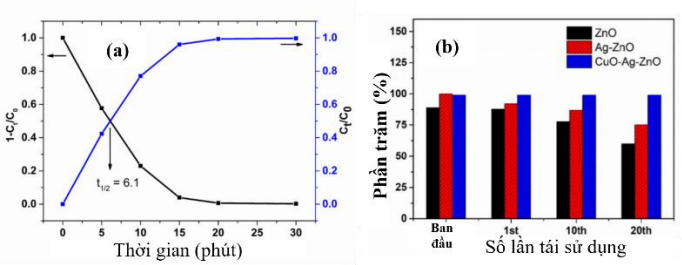

Figure 4 : 7: (a) Half-life estimation curves of MO dyes using CuO-Ag-ZnO NW catalyst materials, and (b) MO reuse studies using ZnO, Ag-ZnO and CuO-Ag - ZnO.

Natural degradation is generally considered to be the half-life, by using CuO-Ag-ZnO NWs as photocatalysts, the half-life of MO was estimated by the intersection of the decomposition yield curve. ($1-C_t/C_0$) and dye concentration (C_t/C_0) over time of illumination. The value of $t_{1/2}$=6,1 min (Figure 4.7 a). This half-life of the CuO-Ag-ZnO NWs is much lower than that of the catalyst samples in previous reports. It should be noted that ZnO is known as an unstable photocatalyst in aqueous media. This disadvantage is significantly overcome in the fabricated tertiary structure. Typically, CuO-Ag-ZnO NWs are used in the 20-fold photodegradation of the dye, and after each run, the CuO-Ag-ZnO NWs are separated from the mixture by centrifugation .

GENERAL CONCLUSION

1. nanowire photocatalyst materials by hydrothermal and photoreduction methods with TiO_2 wire diameter less than 50 nm and Ag particles 10-20 nm in size. Ag/TiO_2 showed an efficient MO decomposition efficiency of 98,8%. In addition, Ag/TiO_2 showed superior photoreduction (50,4 $\mu mol.g^{-1}cat.h^{-1}$) in photoreduction of CO_2 to CH_4 fuel gas .

2. Successfully fabricated TiO_2 co-doped (N, Ta) by hydrothermal method. Co-doped TiO_2 (N, Ta) exhibits high photocatalytic activity in methylene blue degradation with an efficiency of about 93% after 180 min of illumination.

3. Successfully fabricated co-doped modified TiO_2 nanoparticles (N, Ta) with different N content (6%; 7,5%; 9%; 10,5%) by microwave method. The co-doping samples show clearly variable band gap. TiO_2 co-doped (N, Ta) with 7,5% N has high catalytic activity in the photocatalytic reduction of CO_2 to CH_4 gas with a yield of about 7.79 $\mu mol.g^{-1}$ $cat.h^{-1}$.

4. Successfully fabricated ZnO films with Ag and Au nanoparticles attached simultaneously by hydrothermal method and plasma technique. The morphological structure and bandgap properties of the material system are expanded and the ultraviolet emission is strongly enhanced, contributing to changing the photocatalytic activity of the fabricated materials. The Au-Ag-ZnO film with an initial $_{AgNO3}$ precursor concentration of 45mM resulted in superior photodegradation efficiency of 70% RhB.

5. Successfully fabricated the tertiary heterostructure of CuO-Ag-ZnO nanowires by combining a two-step synthesis process including: successfully fabricating ZnO nanowires by hydrothermal method; coating Ag and CuO nanoparticles on the surface of ZnO

nanowires by plasma technique. In the application of decomposition of methyl orange, within the first 15 minutes, the decolorization of methyl orange was 96,3% for CuO-Ag-ZnO and CuO-Ag-ZnO materials with high reaction rate constant k = 0.207 min^{-1} and low half life τ= 6,1 min compared with Ag-ZnO nanowire and ZnO nanowire. At the same time, the study shows that the optical reusability of CuO-Ag-ZnO is much greater than that of ZnO nanowires .

LIST OF WORKS OF THE AUTHOR

1. **Vu Duy Thinh**, VD Lam, TN Bach, ND Van, DH Manh, DH Tung, NTH Lien, UTD Thuy, TX Anh, NT Tung, and NTH Le, Enhanced Optical and Photocatalytic Properties of Au/Ag Nanoparticle-decorated ZnO Films, Journal of ELECTRONIC MATERIALS, Vol. 49, No. 4,2020,2625-2632
2. Phung Thi Thu, **Vu Duy Thinh,** Vu Dinh Lam, Ta Ngoc Bach, Le Thi Hong Phong, Do Hoang Tung, Do Hung Manh, Nguyen Van Khien, Trinh Xuan Anh and Ngo Thi Hong Le, Decorating of Ag and CuO on ZnO nanowires by Plasma Electrolyte Oxidation Method for Enhanced Photocatalytic Efficiency, Catalysts2022, 12.
3. **Vu Duy Thinh**, Vu Dinh Lam, Ta Ngoc Bach, Phung Thi Thu, Le Thi Hong Phong, Do Hung Manh, Ngo Thi Hong Le, Fabrication and photocatalytic property of ZnO nanorod films, 18-20 August, 2021, (IWAMSN2021).
4. **Vu Duy Thinh**, Vu Dinh Lam, Ta Ngoc Bach, Phung Thi Thu, Le Thi Hong Phong, Do Hung Manh, Trinh Xuan Anh, Ngo Thi Hong Le, Synthesis and research on photocatalytic activity and CO2 reduction of Ag/TiO2 nanowires, Vietnam Journal of Catalysis and Adsorption, 10 (2021) 158-162.
5. **Vu Duy Thinh**, Ngo Thi Hong Le "Synthesis and Photocatalytic Activity of (N, Ta) Co-doped TiO_2 Nanopowders", Proceedings of the 12th Asian Conference on Chemical Sensors (ACCS2017),2017, pp.354- 358.
6. Do Khanh Tung, Ta Ngoc Bach, **Vu Duy Thinh,** Do Hung Manh, Vu Dinh Lam, Ngo Thi Hong Le, Research and fabrication of modified TiO_2 nanoparticles to photo-reduce CO_2 into fuel gas. Journal of Science (Hanoi National University of Education2) (2017), no. 52,20